Quantum Monte Carlo study of Doppler broadening of positron annihilation radiation in semiconductors and insulators

K. A. Simula,[1] J. Härkönen,[1] I. Zhelezova,[1] N. D. Drummond,[2] F. Tuomisto,[1] and I. Makkonen[1]

[1] *Department of Physics, P.O. Box 43, FI-00014 University of Helsinki, Finland*
[2] *Department of Physics, Lancaster University, Lancaster LA1 4YB, United Kingdom*

(Dated: April 27, 2023)

The measurement of momentum distribution of positron annihilation radiation in crystalline solids is a powerful method to detect and identify open-volume defects in crystalline solids. The Doppler broadening of the 511-keV line of the 2γ electron-positron annihilation reflects the momentum density of annihilating pairs and local electron momenta at positron annihilation sites. It can provide infomation on the chemical surroundings of vacancies such as the impurity atoms around them. Accurate methods based on first-principles calculations are crucial for interpreting measured Doppler spectra. In this work we will validate such a method based on variational Monte Carlo by benchmarking results in aluminium nitride and silicon against experimental data measured from defect-free reference samples. The method directly models electron-positron correlations with variational wave functions. We achieve better agreement with experiments for our test set than conventional state-of-the-art methods. We show that normalized Doppler broadening spectra calculated with quantum Monte Carlo converge rapidly as a function of simulation cell size, and backflow transformations have a minor effect. This makes the method robust and practical to support positron-based spectroscopies.

I. INTRODUCTION

Positron annihilation spectroscopy is a powerful method for detecting, quantifying and identifying defects in crystalline solids such as metals, alloys semiconductors and complex oxides [1]. In order to determine the atomic and electronic structures responsible for the obtained measurement data, theoretical considerations and computational methods are needed. Accurate calculations require theoretically well defined and practical *ab initio* methods.

So far, the only practical method to support positron experiments of defects is the two-component density-functional theory (DFT) for electron-positron systems [2]. It is a powerful method for modeling solid-state systems with positrons annihilating either from a delocalized state or from trapped states in open-volume defects. However, in addition to the usual exchange-correlation energy one has to approximate and parametrize the electron-positron correlation energy and the so-called enhancement factor needed to include the screening of the positron by electrons when modeling the positron annihilation rate. Momentum-space quantities such as the annihilating-pair momentum density (APMD), directly related to the Doppler broadening of the annihilation radiation, are not well-defined in DFT framework [3]. Instead, approximations are needed, which again are based on parametrized enhancement factors (see, for example [4, 5]). Often the only way to justify the choice of a particular combination of approximations to be used for a given problem is experimental validation [6].

Modelling of correlated densities or momentum space quantities without aforementioned approximations from first principles requires in practice the application of many-body wave function methods [7] or many-body perturbation theory [8]. Thanks to the development of the available computing capacity and methods this is becoming possible. Recently it has been demonstrated for a small benchmark set of systems that quantum Monte Carlo (QMC) calculations based on variational and diffusion Monte Carlo (VMC and DMC) can be used for real inhomogenous periodic solids [9]. The QMC method can predict positron lifetimes of defect-free solids with an accuracy that is on average better than that of existing two-component DFT approximations [9].

In this work, we extend the QMC simulation of positrons to estimation of APMD for the same insulators and semiconductors as in Ref. [9]: C and Si in the diamond structure, as well as wurtzite AlN. Using VMC, we focus on experimental validation of the method's applicability in prediction of the Doppler broadening of the annihilation radiation in AlN and Si. Measurement of the Doppler broadening is the most practical and sensititve method for defect identification but requires a strong theory support for its analysis. Even though we expect the method to work for metals, we exclude them here due to the larger computational cost associated with the increased momentum resolution requirement needed to describe Fermi surface signatures correctly.

By establishing a workflow for VMC simulation of APMD, we study the required accuracy for the wave functions and finite-size effects. Also the vibrational effects on APMD are studied and found to be insignificant. With convergent wave functions and simulation cell sizes, we calculate predictions for the Doppler broadening in Si and AlN, and compare the results against experiments. The comparison shows that our method outperforms DFT-based methods.

Together with the recent milestone of using QMC to accurately predict positron lifetimes in solids [9], this work generalizes the QMC method as a practical tool to support positron-based spectroscopies. Of particu-

lar importance is the finding that, unlike with lifetime calculations, in calculating APMD small simulation cell sizes are convergent and the backflow corrections are not needed. Hence accurate APMD results can be achieved with small computational cost, as opposed to lifetime calculations, where at least the backflow function is needed [9].

Promising future applications can include simulations with positrons trapped at large void-like defects or the study of surface states, where non-local electron-positron correlations dominate and local or semilocal correlation functionals of the two-component DFT fail [10, 11]. These extensions to the applicability of QMC enable it to support positron spectroscopic methods detecting and identifying open-volume defects in crystalline matter [1] or surface-layer sensitive surface techniques such as positron-annihilation induced Auger spectroscopy [12].

II. THEORY AND COMPUTATIONS

In positron annihilation experiments of solids, positrons are implanted in the lattice one at a time. They thermalize rapidly and often trap in open-volume defects before annihilating with an electron. The technique essentially probes the ground state of the electron-positron system. The APMD is reflected in the annihilation γ radiation. The Doppler broadening of the 511-keV annihilation line measures essentially the longitudinal component of the momentum density of annihilating pairs.

We simulate the ground state of inhomogenous crystal lattices with a single thermalized positron using periodic boundary conditions. We use variational Monte Carlo (VMC) method [13] as implemented in the CASINO code [14, 15], with Slater-Jastrow (SJ) and Slater-Jastrow-backflow (SJB) wave functions [16, 17]:

$$\Psi_{\mathrm{SJ}}(\mathbf{R}) = e^{J(\mathbf{R})}\left[\phi^l(\mathbf{r}_{i\uparrow})\right]\left[\phi^m(\mathbf{r}_{j\downarrow})\right]\phi_+(\mathbf{r}_+), \tag{1}$$

$$\Psi_{\mathrm{SJB}}(\mathbf{R}) = e^{J(\mathbf{R})}\left[\phi^l(\mathbf{r}_{i\uparrow}-\boldsymbol{\xi}_{i\uparrow}(\mathbf{R}))\right]\left[\phi^m(\mathbf{r}_{j\downarrow}-\boldsymbol{\xi}_{j\downarrow}(\mathbf{R}))\right] \times \phi_+(\mathbf{r}_+-\boldsymbol{\xi}_+(\mathbf{R})),$$

The SJ wave functions consist of Slater determinants, denoted by [...]-brakets in Eq. (1) and constructed from single-particle Kohn-Sham orbitals ϕ [18]. The determinants are multiplied by a Jastrow factor $\exp(J(\mathbf{R}))$ describing the interparticle correlations. The Jastrow factor consists of parametrized polynomial components describing two-particle, particle-nucleus and 3-body correlations [19]. In the SJB wave functions, the particle coordinates are replaced by quasiparticle coordinates by doing a backflow transformation represented by a parametrized polynomial of interparticle distances.

The single-particle electronic orbitals ϕ are obtained from a DFT simulation using Quantum ESPRESSO [20] and the PBE functional. To obtain the positron orbital we use our own positron package [21].

Before accumulating statistics on momentum densities, we first optimize the Jastrow factor with variance minimization [19], followed by optimization of both the Jastrow factor and backflow transformations by minimizing energy [22]. The parametrizations are consistent with the positron lifetime studies performed in Ref. [9], which also describes in detail how the Slater part of the wave functions are constructed.

Twisted boundary conditions [23] are imposed so that the wave functions obtain a phase in translation of an electron with a simulation cell lattice vector $\mathbf{R}_s$,

$$\Psi_{\mathbf{k}_s}(\mathbf{r}_0,\ldots,\mathbf{r}_i+\mathbf{R}_s,\ldots,\mathbf{r}_N) = \exp(i\mathbf{k}_s\cdot\mathbf{R}_s)\Psi_{\mathbf{k}_s}(\mathbf{r}_0,\ldots,\mathbf{r}_N). \tag{2}$$

Twist offsets $\mathbf{k}_s$ are set in a regular grid in the irreducible wedge of the 1st Brillouin zone of the simulation cells. Regarding translations of the positron, we do not use twisted boundary conditions, since in a usual experimental case we have only one delocalized positron in an infinite lattice at a time, which corresponds physically to a positron orbital with $\mathbf{k}=0$.

Multiple finite-size effects, originating from the finite simulation cell and discrete momentum grid of the wave function, can bias computed energies and positron observables. Kinetic energy bias [24] and the effects from neglecting long-range correlation effects [15] can be reduced with larger simulation cell sizes and twist averaging. Twist averaging is also used to obtain a sufficient momentum resolution in a momentum density calculation. Earlier studies [9] of positron relaxation energies and positron-electron contact pair correlation functions show that 16-atom face-centered cubic simulation cells for C and Si and 16-atom hexagonal cell for AlN with twist grids of $4\times4\times4$ and $4\times4\times5$, respectively, are already fairly convergent. However, we have done further studies on the finite-size effects of APMD and present the results below.

In the case of 2γ annihilation (spin-singlet electron-positron pairs) the APMD corresponds to the net momentum density of the 511-keV annihilation photons. The momentum density for a wave function $\Psi_{\mathbf{k}_s}$ is a set of values $\rho(\mathbf{p}_i)$ on a momentum grid, where $\mathbf{p}_i=\mathbf{k}_s+\mathbf{G}_i$. Here, $\mathbf{G}_i$ are the reciprocal lattice points of the simulation cell. $\rho(\mathbf{p}_i)$ can be computed with

$$\rho(\mathbf{p}_i) = \int d\mathbf{R}\,\Psi^*_{\mathbf{k}_s}(\mathbf{r}_1,\mathbf{r}_1,\ldots,\mathbf{r}_N) \times e^{i\mathbf{p}_i\cdot(\mathbf{r}_0-\mathbf{r}_1)}\hat{O}^s_i\Psi_{\mathbf{k}_s}(\mathbf{r}_0,\mathbf{r}_0,\ldots,\mathbf{r}_N), \tag{3}$$

where $\mathbf{R}=(\mathbf{r}_0,\mathbf{r}_1,\ldots,\mathbf{r}_N)$ is a vector of length $3(N+1)$ containing the coordinates of the positron and N electrons, respectively [25], and $\hat{O}^s_i$ is the spin-projection operator to the singlet-state of the electron-positron pair. In VMC, we propagate the $N+1$ particles using the Metropolis algorithm and sample the APMD using

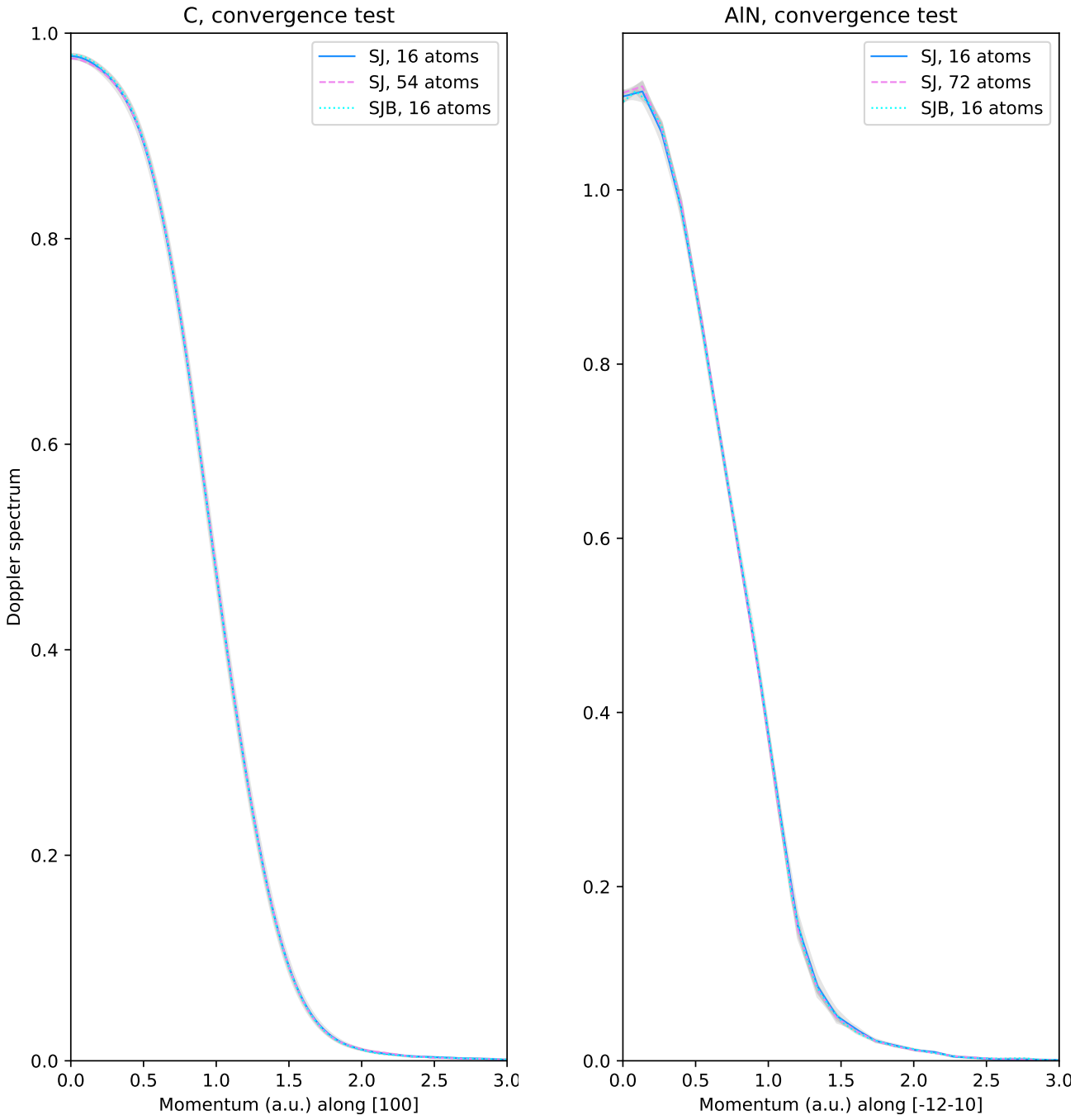

FIG. 1. Unconvoluted Doppler spectra of C (left) and AlN (right) in the [100]- and [–12–10]-directions, respectively. In both materials, the APMD is computed with two different simulation cell sizes (blue: 16-atom cell, violet: 54-atom cell in C and 72-atom cell in AlN) with SJ wave function and with SJB wave function the smaller simulation cell (light blue).

$$\rho(\mathbf{p}_i) = \left\langle \frac{\Psi^*_{\mathbf{k}_s}(\mathbf{r}_1, \mathbf{r}_1, \ldots, \mathbf{r}_N)\hat{O}^s_i \Psi_{\mathbf{k}_s}(\mathbf{r}_0, \mathbf{r}_0, \ldots, \mathbf{r}_N)}{|\Psi_{\mathbf{k}_s}(\mathbf{r}_0, \mathbf{r}_1, \ldots, \mathbf{r}_N)|^2} e^{i\mathbf{p}_i\cdot(\mathbf{r}_1-\mathbf{r}_0)} \right\rangle_{|\Psi_{\mathbf{k}_s}|^2} . \quad (4)$$

The averaging involves in practice also a permutation over opposite spin electron indices.

The accumulation of APMD as in Eq. (3) can only be done in the VMC level, as it involves the estimation of ratios involving wave functions of the SJ or SJB forms. If we used DMC to sample the electronic configurations, we would nevertheless need to use these wave functions in estimation of the ratios, making the DMC accumulation of the operator in Eq. (3) ill-defined. DMC estimation of APMD would be possible by calculating the positron-electron density matrix and using certain off-diagonal parts, but this is outside the scope of this work. Our results show that VMC accumulation of APMD with $\rho(\mathbf{p}_i)$ computed as in Eq. (3) gives sufficient accuracy at least for the bulk materials studied here.

The grid of momentum density values is limited by a suitable cutoff value, so that $|\mathbf{p}_i| < p_{cut}$. In the VMC simulations, we chose $p_{cut} = 7$ a.u., but found the APMD projections to be convergent with already values of ~ 5 a.u.. As mentioned, twist averaging is used to increase the momentum resolution of our APMD estimates. This means that with N_s symmetrically inequivalent twists we must construct N_s wave functions and estimate APMD for each in an independent simulation. However, we have optimized the Jastrow factor only in the Γ-point twist.

We calculate 1D Doppler projections from the 3D APMDs as

$$\rho(p_L) = \int\int dp_x dp_y \rho(\mathbf{p}), \tag{5}$$

where p_L is the longitudinal momentum component of the annihilation photons and the projection is made over the orthogonal plane, by first filling the momentum grid by non-intersecting tetrahedra with a Delaunay tetrahedralization algorithm [26]. Then, the projected $\rho(p_L)$ values are computed with a linear interpolation algorithm [27]. The analysis of statistical error is based on treating the twists $\mathbf{k}_s$ as independent measurements. Before comparing with experiment, the computed Doppler spectra are convoluted with the appropriate experimental resolution function.

Norm-conserving, nonlocal Dirac-Fock average relativistic effective pseudopotentials (AREP)[28] are used to approximate the ion cores. Thus the obtained VMC momentum densities include only the contribution from the valence electrons. We compute the core electron Doppler projections and their relative intensity as compared to total spectra with density functional theory (DFT) based methods. In the calculation of core spectra, we assume core orbitals of free atoms, and the shape of the positron orbital close to the nucleus is parametrized using linear-muffin-tin-orbital calculations [6]. The core spectra are calculated by using either the state-dependent model [5] or the state-independent model [4], and the LDA positron correlation potential and enhancement factor [2]. To estimate the total Doppler spectra with VMC we add the core electron projections to the QMC projection, resulting in our final estimates as $\rho(p_L) = (1-\mu)\rho_{\mathrm{val}}(p_L) + \mu\rho_{\mathrm{core}}(p_L)$, where μ is the relative intensity of the core annihilation according to DFT. An alternative approach of estimating μ is to estimate the valence and core annihilation rates using QMC and DFT, respectively (see Ref. [9]), but this gave only insignificant changes to the final results.

In addition to comparing our VMC result with experiments, we model the APMDs using more conventional density-functional-based calculations and enhancement models for the APMD. We use the VASP code [29] and the projector augmented wave method [30] within the LDA [31] for Si and GGA [32] for C and AlN. We use the electron-positron LDA [2] and both state-dependent [5] and -independent models within LDA [4] for the APMD for comparison, reconstructed PAW orbitals [6, 33] and treating the core elecrons as described above, for evaluating the Doppler spectra.

We also use DFT to estimate the effect of lattice vibrations to APMD in bulk Si. In a 64-atom simulation cell, we solve the phononic modes at Γ point and sample a set of atomic displacements with respect to the equilibrium structure, distributed according to the vibrational modes in 0 and 300 K. Then we construct a set of simulation cells based on the sampled atomic displacements and estimate the APMD in each of the cells. This gives us APMD estimates distributed according to lattice vibrations in the two different temperatures. The method of sampling the atomic displacements was similar to the one used in Ref. [9], but here we used an algorithm implemented in VASP [34]. It should be noted that this method does not include the anharmonic effects.

III. EXPERIMENTAL

We benchmark our simulations agains experimental Doppler broadening data for defect-free Si, AlN and diamond.

The reference Si measurement [35] was performed using a slow positron beam and 2D coincidence Doppler setup with two HPGe detectors with a combined energy resolution of 0.92 keV full width at half maximum (FWHM). The measurement is made from the substrate of a (100) Si:Sb sample using a 20 keV beam energy. We have confirmed the measurement direction $\mathbf{p}_L$ used in the original experiment by an X ray diffraction measurement. It turns out, that instead of the original assumption [35] the cleavage plane of the sample's sides is (110) instead of (100) and thereby the measurement direction of the Doppler experiment is [110].

The AlN reference measurement [36] is also a 2D coincidence Doppler measurement performed using a slow positron beam, with a FWHM of 0.9 keV. The sample's growth direction is the c-axis direction [0001]. The precise alignment of the sample in the measurement is unknown and thereby we only can tell that the $\mathbf{p}_L$ direction is perpendicular to the c-axis, and we choose the direction of Doppler broadening spectrum as [–12–10]. However, the Doppler spectra of AlN are very isotropic in this plane and therefore the precise choice of the projection

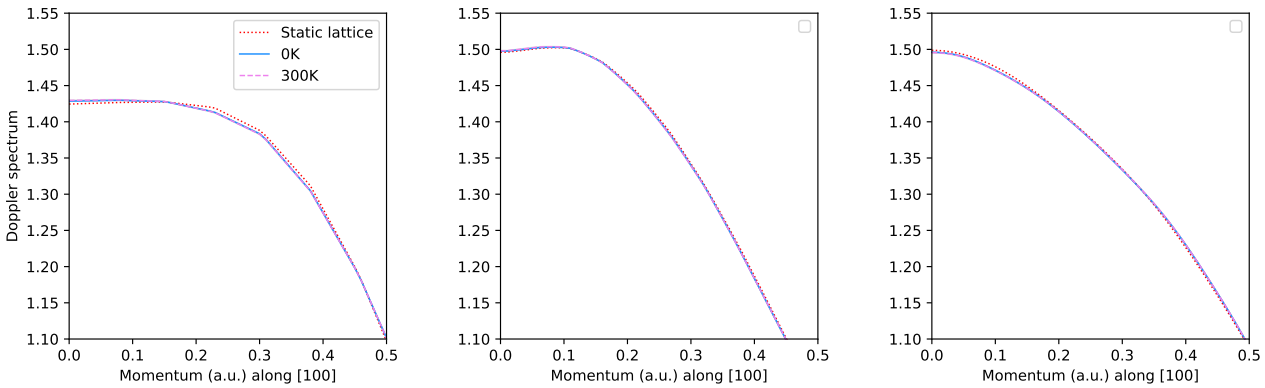

FIG. 2. Doppler spectra of Si along the [100] (left), [110] (middle), and [111] (right) lattice directions from static lattice (red), as compared against vibrationally renormalized projections in 0 (blue) and 300K (violet).

direction in simulations plays only a minor role.

IV. RESULTS AND DISCUSSION

A. Convergence with respect to system size and wave function

Figure 1 shows APMD results from VMC simulations in C and AlN projected in in [100]- and [-12-10]-directions, respectively, according to Eq. (5). The results are obtained using SJ wave functions in 16- and 54-atom (64- and 216-electron) simulation cells in C and 16- and 72-atom (64- and 288-electron) simulation cells in AlN. Also results from SJB simulations in 16-atom simulation cells are shown. Inspection of the different spectra in each of the materials show that the results obtained with different cell size and wave function are within each others' errorbars, and hence we can treat the SJ results in the smaller cells converged. Same conclusions were obtained from APMD calculations in Si.

B. The effect of lattice vibrations in Si

Figure 2 shows the Doppler spectra along the [100]-, [110], and [111]-directions in the Si lattice, computed in DFT level for the static lattice which are compared against the vibrationally renormalized projections in 0 and 300K. Only the projection values at low-momentum regions are shown, as at higher momenta the static and vibrationally renormalized spectra in both temperatures were overlapping with respect to the statistical error.

It can be seen that there is not much effect due to vibrations on the APMD projections. The effect is the same in 0 and 300K. The effect is largest in the [100]-direction, but small when compared against the discrepancies between DFT and QMC, or between DFT and experiment, see below. Furthermore, when comparing against experimental Doppler spectra the convolution of the theoretical projections with the resolution function of the detectors used in measurements makes the effect even smaller. Anharmonic effects in non-zero temperatures are not studied, but thermal expansion can have minor effects.

C. Benchmark against experiments and model calculations

We now compare our results against the 2D coincidence beam measurements for Si [35] and AlN [36]. These experimental references were the best currently available, and further data for e.g. diamond was too noisy to have meaningful theory-experiment comparisons for drawing conclusions on whether DFT or QMC methods provide better results.

1. Si

Figure 3 shows a comparison of the low- and high-momentum regions of the Doppler specrum between VMC, DFT models and the experimental reference [35]. The low- and high-momentum regions are determined mainly by valence and core electrons, respectively. The high-momentum region contains also information relevant for identifying atom types around annihilation sites.

At low momenta we find that the VMC result agrees with experiment within statistic error bars. At higher momenta the agreement remains good, but at momentum higher than $p = 2.5$ a.u the core spectra, calculated with DFT, start to dominate the results and the statistical error of the VMC results starts to be large when compared against the projection values. The choice of the correlation model used for the core electrons of Si does not play a role in this momentum range where we can reliably compare experiment and theory ($p < 2.5$ a.u.).

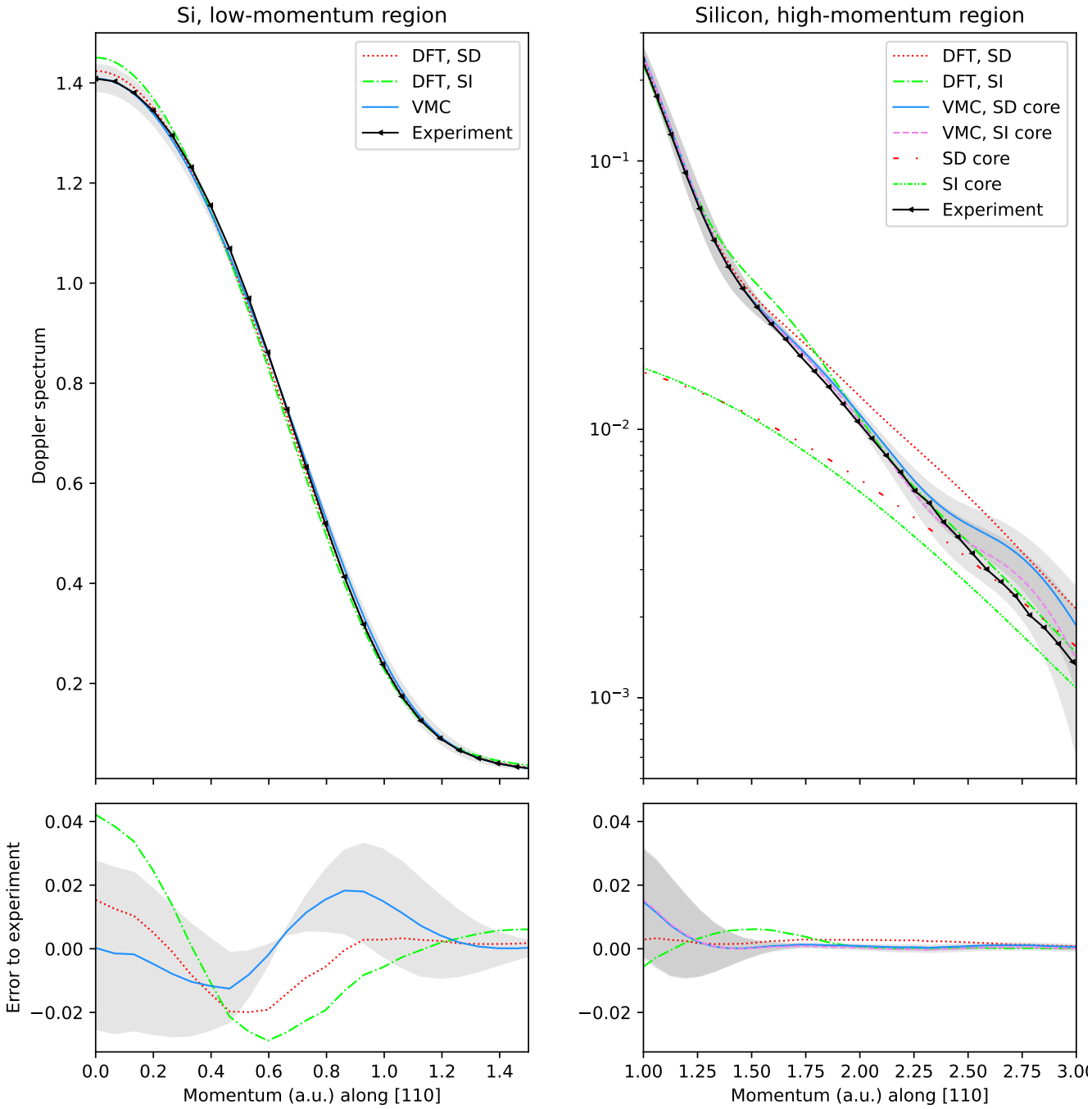

FIG. 3. The low- and high-momentum parts (in left and right, respectively) of the Si Doppler spectrum along the [110] direction. The data includes the experimental benchmark result [35] (black), our VMC data (blue, and violet when state-independent (SI) core spectrum is used), and for comparison DFT-based results calculated by the state-dependent (SD, red) and state-independent (pink) models. The core spectrum obtained from these models and used also in QMC is shown separately. In the left, the SD core spectrum was added to the QMC valence spectrum, in the right, QMC with both core spectra is shown.

Figure 3 shows that the agreement of the DFT-based models (state-dependent and -independent, both applied with Boroński-Nieminen LDA) with experiment is worse than that of VMC, and the results do not lie within statistical error bars. The list of models compared with here is not exhaustive, but the point in this comparison is that the spread between these two results gives an idea of the typical error due to the choice of the correlation model and functional behind the calculation. We want to stress that concerning the enhancement factor parametrizations

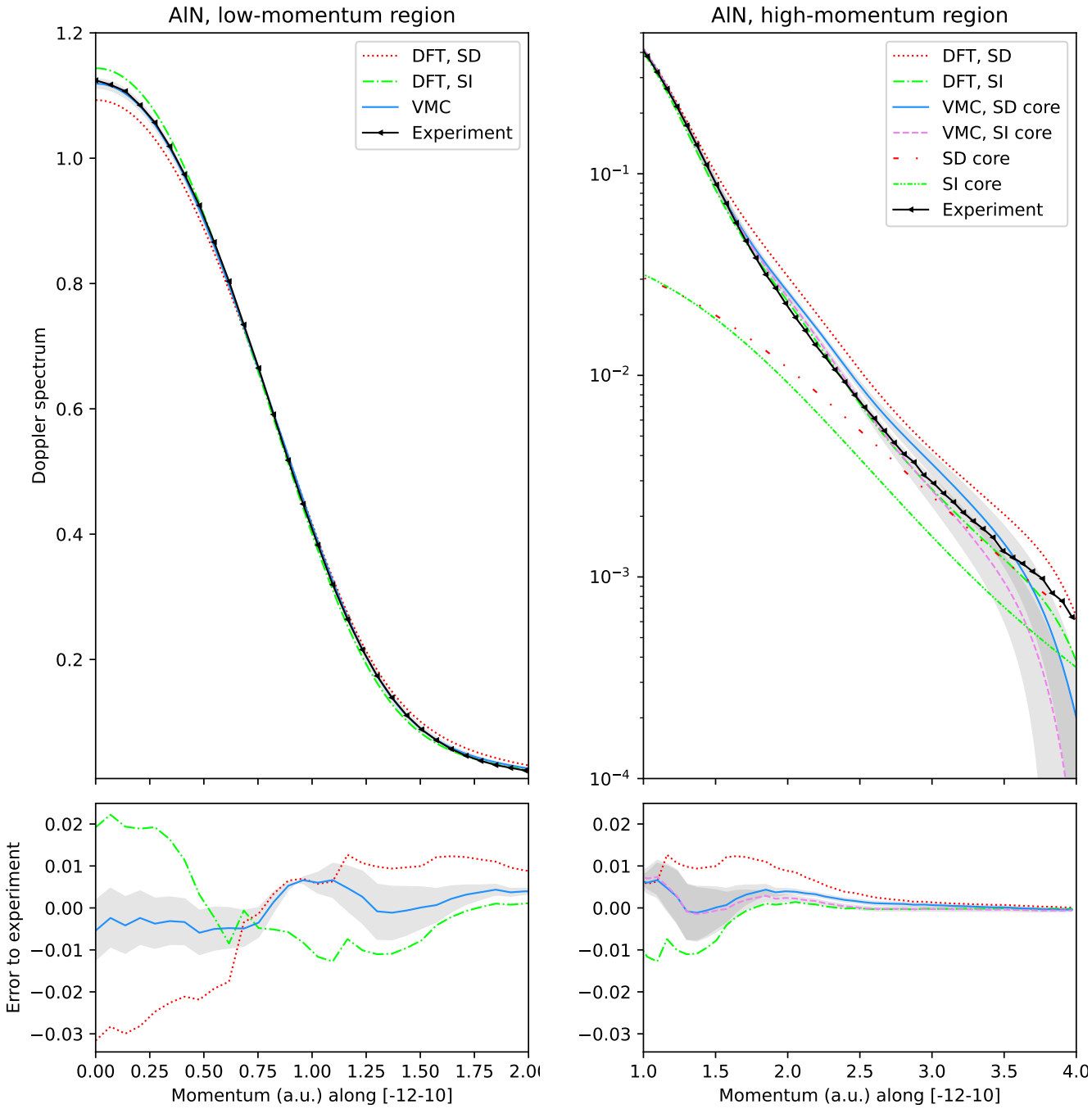

FIG. 4. The low- and high-momentum parts (in left and right, respectively) of the AlN Doppler spectrum along the [-12-10] direction. The data includes the experimental benchmark result [36] (black), our VMC data (blue, and violet when state-independent (SI) core spectrum is used), and for comparison the DFT-based results calculated by the state-dependent (SD, red) and state-independent (pink) models. The core spectrum obtained from these models and used also in QMC is shown separately. In the left, the state-dependent core spectrum was added to the QMC valence spectrum, in the right, QMC with both core spectra is shown.

in the literature, only the various LDA parametrizations (see, for example. Refs. [2, 7]) and a single generalized gradient model [37] are genuinely parameter-free.

At low momenta the state-dependent model agrees better with experiment and VMC, whereas at higher momenta its well-known overestimation of intensity [6] when applied within LDA is apparent and the state-independent model provides a better agreement.

2. AlN

Similar comparison as above for Si is done in Fig. 4. The VMC result displays a formidable agreement with the experimental reference [36], whereas the DFT-based model calculations deviate from the experiment and the VMC result. At high momenta the model used for the core plays a larger role here, as the deviation between core spectra of the state-dependent and -independent models is larger than in Si. The state-independent model gives a better agreement with experiment than state-dependent.

Concerning the DFT-based models, at low momenta both state-dependent and state-independent models perform equally with opposite errors. At high momenta we again see the typical overestimation of the state-dependent model and the LDA.

V. CONCLUSIONS

In this work, a VMC study for computing annihilating-pair momentum densitites in insulator and semiconductor materials was presented. Same methods as in this study can be applied in metals, but this requires a more accurate sampling of the momentum grid, meaning one should have a larger simulation cell or a denser twist grid. The VMC results were compared against state-dependent and state-independent models in the framework of DFT and against experimental Doppler broadening measurements.

The convergence with respect to simulation cell size was tested. It was found that backflow is not necessary for obtaining accurate and convergent results. Also we tested the effect of lattice vibrations to APMD, and found that it is sufficient to consider a static lattice with equilibrium atomic structure. These tests show that it is possible to perform accurate VMC calculations for APMD with relatively low computational costs.

The VMC results match better with experimental Doppler broadening spectra than results from the previous DFT-based methods. This shows how explicit inclusion of the electron-electron and electron-positron correlation effects can be used to improve the correspondence of experiment and theory in positron-based spectroscopies. With the previous QMC results for positron lifetimes in solids this article shows how QMC can be used as a practical tool to support positron spectroscopies when high accuracy is needed.

A recent study [38] shows how the same method that is capable to predict positron lifetimes and Doppler broadening spectra accurately can be utilized in capturing correlations of the nitrogen-vacancy center in diamond. Thus we expect the method used here and for the lifetimes in Ref. [9] to be applicable for simulations of positrons trapped at open-volume defects. This, among other promising routes such as simulation of positrons at surfaces or interfaces, shows potential for very interesting applications of positron spectroscopies supported by QMC simulations.

[1] F. Tuomisto and I. Makkonen, Defect identification in semiconductors with positron annihilation: Experiment and theory, Rev. Mod. Phys. **85**, 1583 (2013).

[2] E. Boroński and R. M. Nieminen, Electron-positron density-functional theory, Phys. Rev. B **34**, 3820 (1986).

[3] I. Makkonen, M. M. Ervasti, T. Siro, and A. Harju, Enhancement models of momentum densities of annihilating electron-positron pairs: The many-body picture of natural geminals, Phys. Rev. B **89**, 041105 (2014).

[4] S. Daniuk, G. Kontrym-Sznajd, A. Rubaszek, H. Stachowiak, J. Mayers, P. A. Walters, and R. N. West, Selective enhancement of different electron populations by electron-positron attraction: application to zinc, J. Phys. F: Met. Phys. **17**, 1365 (1987); T. Jarlborg and A. K. Singh, Local-density approach for calculation of electron-positron enhancement in transition metals, Phys. Rev. B **36**, 4660 (1987).

[5] M. Alatalo, B. Barbiellini, M. Hakala, H. Kauppinen, T. Korhonen, M. J. Puska, K. Saarinen, P. Hautojärvi, and R. M. Nieminen, Theoretical and experimental study of positron annihilation with core electrons in solids, Phys. Rev. B **54**, 2397 (1996).

[6] I. Makkonen, M. Hakala, and M. J. Puska, Modeling the momentum distributions of annihilating electron-positron pairs in solids, Phys. Rev. B **73**, 035103 (2006).

[7] N. D. Drummond, P. López Ríos, R. J. Needs, and C. J. Pickard, Quantum monte carlo study of a positron in an electron gas, Phys. Rev. Lett. **107**, 207402 (2011).

[8] J. Hofierka, B. Cunningham, C. M. Rawlins, C. H. Patterson, and D. G. Green, Many-body theory of positron binding to polyatomic molecules, Nature **606**, 688 (2022).

[9] K. A. Simula, J. E. Muff, I. Makkonen, and N. D. Drummond, Quantum Monte Carlo study of positron lifetimes in solids, Phys. Rev. Lett. **129**, 166403 (2022).

[10] W. Shi, V. Callewaert, B. Barbiellini, R. Saniz, M. Butterling, W. Egger, M. Dickmann, C. Hugenschmidt, B. Shakeri, R. W. Meulenberg, E. Brück, B. Partoens, A. Bansil, and S. W. H. Eijt, Nature of the positron state in cdse quantum dots, Phys. Rev. Lett. **121**, 057401 (2018).

[11] Q. Yang, Z. Hu, I. Makkonen, P. Desgardin, W. Egger, M.-F. Barthe, and P. Olsson, A combined experimental and theoretical study of small and large vacancy clusters in tungsten, Journal of Nuclear Materials **571**, 154019 (2022).

[12] V. Chirayath, V. Callewaert, A. Fairchild, M. Chrysler, R. Gladen, A. Mcdonald, S. Imam, K. Shastry, A. Koymen, R. Saniz, *et al.*, Auger electron emission initiated by the creation of valence-band holes in graphene by positron annihilation, Nature communications **8**, 16116 (2017); A. J. Fairchild, V. A. Chirayath, R. W. Gladen, A. R. Koymen, A. H. Weiss, and B. Barbiellini, Pho-

toemission spectroscopy using virtual photons emitted by positron sticking: A complementary probe for top-layer surface electronic structures, Phys. Rev. Lett. **129**, 106801 (2022).
[13] W. M. C. Foulkes, L. Mitas, R. J. Needs, and G. Rajagopal, Quantum monte carlo simulations of solids, Rev. Mod. Phys. **73**, 33 (2001).
[14] R. J. Needs, M. D. Towler, N. D. Drummond, and P. López Ríos, Continuum variational and diffusion quantum Monte Carlo calculations, J. Phys.: Condens. Matter **22**, 023201 (2009).
[15] R. J. Needs, M. D. Towler, N. D. Drummond, P. López Ríos, and J. R. Trail, Variational and diffusion quantum Monte Carlo calculations with the CASINO code, J. Chem. Phys. **152**, 154106 (2020).
[16] R. Jastrow, Many-body problem with strong forces, Phys. Rev. **98**, 1479 (1955).
[17] P. López Ríos, A. Ma, N. D. Drummond, M. D. Towler, and R. J. Needs, Inhomogeneous backflow transformations in quantum monte carlo calculations, Phys. Rev. E **74**, 066701 (2006).
[18] W. Kohn and L. J. Sham, Self-consistent equations including exchange and correlation effects, Phys. Rev. **140**, A1133 (1965).
[19] N. D. Drummond, M. D. Towler, and R. J. Needs, Jastrow correlation factor for atoms, molecules, and solids, Phys. Rev. B **70**, 235119 (2004).
[20] P. Giannozzi, O. Baseggio, P. Bonfà, D. Brunato, R. Car, I. Carnimeo, C. Cavazzoni, S. De Gironcoli, P. Delugas, F. Ferrari Ruffino, *et al.*, Quantum espresso toward the exascale, The Journal of Chemical Physics **152**, 154105 (2020).
[21] T. Torsti, T. Eirola, J. Enkovaara, T. Hakala, P. Havu, V. Havu, T. Höynälänmaa, J. Ignatius, M. Lyly, I. Makkonen, *et al.*, Three real-space discretization techniques in electronic structure calculations, Phys. Status Solidi (b) **243**, 1016 (2006).
[22] C. J. Umrigar, J. Toulouse, C. Filippi, S. Sorella, and R. G. Hennig, Alleviation of the fermion-sign problem by optimization of many-body wave functions, Phys. Rev. Lett. **98**, 110201 (2007).
[23] C. Lin, F. H. Zong, and D. M. Ceperley, Twist-averaged boundary conditions in continuum quantum monte carlo algorithms, Phys. Rev. E **64**, 016702 (2001).
[24] M. Holzmann, R. C. Clay, M. A. Morales, N. M. Tubman, D. M. Ceperley, and C. Pierleoni, Theory of finite size effects for electronic quantum monte carlo calculations of liquids and solids, Phys. Rev. B **94**, 035126 (2016).
[25] G. Ryzhikh and J. Mitroy, Positron annihilation profiles for hps and he (3se) e+, Journal of Physics B: Atomic, Molecular and Optical Physics **32**, 4051 (1999).
[26] J. R. Shewchuk, Lecture notes on Delaunay mesh generation (1999).
[27] M. Matsumoto, M. Tokii, and S. Wakoh, An improvement of the linear tetrahedron method for Compton profile calculations, J. Phys. Soc. Jpn **73**, 1870 (2004).
[28] J. R. Trail and R. J. Needs, Norm-conserving Hartree–Fock pseudopotentials and their asymptotic behavior, J. Chem. Phys. **122**, 014112 (2005); Smooth relativistic Hartree–Fock pseudopotentials for H to Ba and Lu to Hg, J. Chem. Phys. **122**, 174109 (2005).
[29] G. Kresse and J. Furthmüller, Efficiency of ab-initio total energy calculations for metals and semiconductors using a plane-wave basis set, Computational Materials Science **6**, 15 (1996); G. Kresse and J. Furthmüller, Efficient iterative schemes for ab initio total-energy calculations using a plane-wave basis set, Phys. Rev. B **54**, 11169 (1996).
[30] P. E. Blöchl, Projector augmented-wave method, Phys. Rev. B **50**, 17953 (1994); G. Kresse and D. Joubert, From ultrasoft pseudopotentials to the projector augmented-wave method, Phys. Rev. B **59**, 1758 (1999).
[31] J. P. Perdew and A. Zunger, Self-interaction correction to density-functional approximations for many-electron systems, Phys. Rev. B **23**, 5048 (1981).
[32] J. P. Perdew, K. Burke, and M. Ernzerhof, Generalized gradient approximation made simple, Phys. Rev. Lett. **77**, 3865 (1996).
[33] I. Makkonen, M. Hakala, and M. Puska, Calculation of valence electron momentum densities using the projector augmented-wave method, J. Phys. Chem. Solids **66**, 1128 (2005).
[34] F. Karsai, M. Engel, E. Flage-Larsen, and G. Kresse, Electron–phonon coupling in semiconductors within the gw approximation, New Journal of Physics **20**, 123008 (2018).
[35] M. Rummukainen, I. Makkonen, V. Ranki, M. J. Puska, K. Saarinen, and H.-J. L. Gossmann, Vacancy-impurity complexes in highly sb-doped si grown by molecular beam epitaxy, Phys. Rev. Lett. **94**, 165501 (2005).
[36] J.-M. Mäki, I. Makkonen, F. Tuomisto, A. Karjalainen, S. Suihkonen, J. Räisänen, T. Y. Chemekova, and Y. N. Makarov, Identification of the V_{al}-$\mathrm{O_n}$ defect complex in aln single crystals, Phys. Rev. B **84**, 081204 (2011).
[37] B. Barbiellini and J. Kuriplach, Proposed parameter-free model for interpreting the measured positron annihilation spectra of materials using a generalized gradient approximation, Phys. Rev. Lett. **114**, 147401 (2015).
[38] K. Simula and I. Makkonen, Calculation of the energies of the multideterminant states of the nitrogen vacancy center in diamond with quantum monte carlo, arXiv preprint arXiv:2303.09851 https://doi.org/10.48550/arXiv.2303.09851 (2023).